Finding the Center of a Phyllotactic Pattern*

Scott Hotton

Department of Mathematics and Statistics, Miami University, Oxford, OH 45056

Abstract: The calculation of divergence angles between primordia in a plant apex depends on the point used as the center of the apex. In mathematically ideal phyllotactic patterns the center is well defined but there has not been a precise definition for the center of naturally occurring phyllotactic patterns. A few techniques have been proposed for estimating the location of the center but without a precise definition for the center the accuracy of these methods cannot be known. This paper provides a precise definition that can be used as the center of a phyllotactic pattern and a numerical method which can accurately find it. These tools will make it easier to compare theory against experiment in phyllotaxis.

1. Introduction

It is well known that plant organs tend to form regular patterns and that the study of these patterns is called phyllotaxis. Most plant organs develop from meristematic tissue in plant apices called the *shoot apical meristem* (SAM). Extensive cell divisions along the boundary of the meristems produce primordia which develop into various plant organs. The pattern exhibited by the collection of primordia is preserved as they develop.

Phyllotactic patterns do not form all at once but rather in a sequential order. To understand how a particular pattern arises we need to understand its ontogeny. This calls for a dynamical model of meristematic development. To compare a dynamical model with a developing apex we want to observe each primordium form. Primordia are tiny and can only be precisely observed under a microscope. The instrument of choice is the scanning electron microscope (SEM). Optical microscopes lack the depth of field needed to get well focused images. Unfortunately the act of observing an SAM under an SEM disturbs its growth. To get around this difficulty techniques based on making molds of a shoot apex as it grows have been developed (see (Williams & Green 1988), (Hernandez *et al.*, 1991), (Hill, 2001), (Dumais & Kwiatkowska, 2002)).

Spiral phyllotaxis is characterized by the presence of two sets of distinctive spiral rows of botanical units. The spirals are called *parastichies*. One set of parastichies coils in the opposite direction from the other. The pair of numbers that enumerate how many parastichies are in each set are called the *parastichy numbers*. The parastichy numbers are often successive Fibonacci numbers.

Another important quantity characterizing a phyllotactic pattern is the *divergence angle, i.e.* the angle between primordia that form consecutively. This angle often varies only slightly about some particular value as the plant develops. In distichous phyllotaxis the divergence angle is about 180^o while in spiral phyllotaxis it is usually about 137.5^o. The Bravais brothers (Bravais & Bravais, 1837) showed that the parastichy numbers of a spiral lattice with a divergence angle close to 137.5^o are consecutive Fibonacci numbers.

Hofmeister (Hofmeister, 1868) performed one of the first microscopic studies of shoot apices. From his observations he proposed a set of hypothesis for SAM ontogeny. Dynamical models (Atela *et al.*, 2002), (Douady & Couder, 1996) based on Hofmeister's hypothesis lead to distichous patterns and to spiral lattices with a divergence angle of about 137.5^o. So there is nice congruence between theory and fact.

* Supplementary appendices are available at doi:00000000000000000000000000000.

It is often convenient to assume the apex is circularly symmetric. While this is a useful approximation real plant apices often deviate noticeably from perfect circular symmetry. There are an endless variety of shapes that plant apices can assume *e.g.* ellipsoidal, polygonal, or hourglass shaped. Furthermore the parastichies are not always strictly spiral shaped. Sometimes they can undulate. Also real phyllotactic patterns exhibit dislocations and the parastichy numbers can sometimes be off by one or two from a Fibonacci number especially when the parastichy numbers are large. So a more detailed analysis of plant patterns is necessary to connect theory with fact.

This paper is about finding a good point on an apical surface to calculate divergence angles from. Not surprisingly it turns out that the problem of finding this point in a naturally occurring phyllotactic pattern depends on how we define it. This is discussed in section 2. To deal with real phyllotatic patterns we need some way of defining the center that is general enough to deal with the diversity of phyllotatic patterns. In section 3 we introduce the concept of the "minimal variation center". It provides an objective and reasonable way to deal with this diversity. Sections 4 and 5 provide an algorithm for finding the minimal variation center and illustrate its usage with some examples.

Plants generate primordia in a precise fashion producing the crystalline like phyllotactic patterns we see in many specimens. Even when the pattern we see in a particular plant is not as perfect as we would like we should not assume that primordia formation is not as precisely determined by the plant as it is in more ideal specimens. To learn how plants use positional information in more general situations we need to measure the positions of primordia as precisely as possible.

To obtain positional data on morphological forms certain features are usually selected to mark their location. For example in members of the Asteraceae family disk floret primordia often display a five-pointed star shaped invagination when the petals begin to form. The center of this star can be used as a marker for the position of the floret primordia. More often young primordia tend to have fairly smooth surfaces and lack distinctive features that can be use as markers. This has made it difficult to measure primordia position precisely. We can choose a point on the surface of a young primordium which appears to be the furthest above the surrounding meristem surface to be a marker for the primordium's position. In many cases young primordia are approximately hemispherical. In these cases we can choose a point which is about equidistant to the perceived boundary of the primordium to be the marker. Since primordia are not all exactly the same shape the various methods for choosing a marker are not entirely consistent with one another. Currently we cannot be confident that measurements of primordia location have the same degree of precision as the process which generated them. In section 6 we show how the minimal variation center can also be used to reduce the impact uncertainties in primordia position have on the computation of divergence angles. Section 7 will illustrate this with four examples.

It is easier to obtain precise measurements of primordia location when the apices are fairly flat like those from the Asteraceae family. The flowering shoots in this family are often referred to as *capitula*. In these capitula an observer can work from a single micrograph which one tries to take as parallel to the surface as possible. Most apices, though, are dome shaped and the primordia form a three dimensional configuration. There are fairly accurate methods for obtaining three dimensional data from plant apices (see (Williams, 1975) and (Dumais & Kwiatkowska, 2002)) but they are not widely used. This paper will focus mainly on how to analyze apices that are approximately flat.

While the center of a two dimensional pattern is a point the center of a three dimensional pattern is a curve. In a circularly symmetric apex this curve is a straight line and even without circular symmetry the center can still be a straight line. Section 8 will discuss how to find this line. There are instances, however, where a plant shoot does not grow in a straight manner (for examples see (Sattler, 1973)). These cases

are much more complicated and will have to be dealt with in a further paper.

2. Previous Methods for Finding the Center

Let's consider some methods that have been employed in the past to find the center of phyllotactic patterns. This is not a review of all possible methods that have been used. Rather we are only choosing some of the simpler methods to highlight the limitation of *ad hoc* approaches. This should help clarify the need for the more systematic approach presented in the following sections. We shall apply the methods of this section to two configurations. The first configuration will be a mathematically ideal pattern while the second configuration will be a randomly perturbed version of the first one.

We'll begin by describing the form of an equiangular spiral lattice. This is a discrete set of points sitting on an equiangular spiral (see figure 1). Mathematically the center is easy to define for this pattern. We simply follow the spiral inward and (in the limit) it will take us there. The divergence angle is the angle between consecutive lattice points along the spiral. This angle is computed from the center of the spiral and it is the same between any two consecutive lattice points. We will denote the divergence angle by δ. The *plastochron ratio* is the ratio of the distances between the center and two consecutive lattice points. This is also the same for any pair of consecutive lattice points in an equiangular spiral lattice. We will denote the plastochron ratio by a.

Given the position of three consecutive points in an equiangular spiral lattice we can derive the plastochron ratio, divergence angle, and the center of the spiral lattice using the properties of similar triangles (see supplementary appendix A*). Let the coordinates of the three consecutive lattice points be (X_1, Y_1), (X_2, Y_2), (X_3, Y_3) where (X_1, Y_1) is the outermost and (X_3, Y_3) is the innermost. And let (x_c, y_c) be the coordinates for the center of the spiral lattice. The

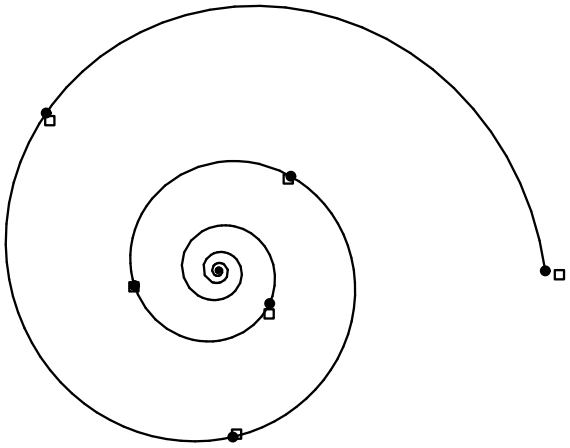

Figure 1: An equiangular spiral and two configurations. The spiral lattice, Pattern C, is indicated by the solid dots. Pattern C' is indicated by the open boxes.

plastochron ratio is given by:

$$a = \sqrt{\frac{(X_2 - X_1)^2 + (Y_2 - Y_1)^2}{(X_3 - X_2)^2 + (Y_3 - Y_2)^2}}$$

The divergence angle is

$$\begin{aligned}\delta = &\text{atan2}(Y_3 - Y_2, X_3 - X_2) \\ &-\text{atan2}(Y_2 - Y_1, X_2 - X_1)\end{aligned}$$

The atan2 function is explained in supplementary appendix B*. Define the four quantities:

$$x_\pm = \frac{(a\cos(\delta) - 1)(X_3 - X_2) \pm a\sin(\delta)(Y_3 - Y_2)}{1 + a^2 - 2a\cos(\delta)}$$
$$y_\pm = \frac{(a\cos(\delta) - 1)(Y_3 - Y_2) \pm a\sin(\delta)(X_3 - X_2)}{1 + a^2 - 2a\cos(\delta)}$$

and the pair of points:

$$((x_+) + X_3, (y_-) + Y_3)$$
$$((x_-) + X_3, (y_+) + Y_3)$$

When $\delta = 0^o$ or $\delta = 180^o$ these two points are actually the same and are equal to (x_c, y_c) (the case $\delta = 0^o$ doesn't resemble a phyllotactic pattern but the case $\delta = 180^o$ is quite common). When $\delta \neq 0^o$ and $\delta \neq 180^o$ these are two distinct points and only one of them is (x_c, y_c). The

	Mathematically Ideal Pattern		Realistic Pattern	
	Outer Triplet	Inner Triplet	Outer Triplet	Inner Triplet
P_1	(40.496,0.0)	(8.9840,11.708)	(42.239,-0.49173)	(8.6569,11.379)
P_2	(-21.326,19.542)	(-10.381,-1.8305)	(-20.873,18.595)	(-10.450,-1.9776)
P_3	(1.8007,-20.582)	(6.3503,-4.0456)	(2.2537,-20.230)	(6.2918,-5.3393)
a	1.4000	1.4000	1.4590	1.3652
δ	137.50^o	137.50^o	137.61^o	133.69^o
(x_c, y_c)	(0.00000,0.00000)	(0.00000,0.00000)	(0.38883,-0.65946)	(0.14202,-0.48471)

Table 1: Results from the triplets of lattice points shown in figure 1. The calculations were done to ten digits and have been rounded to five digits in the table.

correct choice can be made by inspection of the figure. A formal procedure to make the correct choice is in supplementary appendix A*.

We shall call this the *three-point* method. Maksymowych & Erickson (Maksymowych & Erickson, 1977) derived the same formula for a and a formula like the one here for δ. Meicenheimer expanded on their work to derive a formula similar to the one here for the coordinates of the center which he applied to *Linum* shoot apices (Meicenheimer, 1986).

In this mathematically ideal situation it does not matter which three consecutive points of the equiangular spiral lattice we use - we will get the same value for the center. For example consider the equiangular spiral lattice in figure 1. This spiral lattice resembles a commonly seen phyllotactic pattern. Its plastochron ratio is 1.4, its divergence angle is 137.5^o and the center is located at $(0, 0)$. The positions of the lattice points are

$$x_j = 1.4^{(12-j)} \cos(137.5^o(j-1))$$
$$y_j = 1.4^{(12-j)} \sin(137.5^o(j-1))$$

where $j = 1, \ldots, 6$. We'll shall call this configuration "pattern C".

In this demonstration we select two distinct triplets of consecutive lattice points from this spiral lattice. In particular we choose the outer most triplet

$$\begin{aligned}(X_1, Y_1) &= (x_1, y_1)\\ (X_2, Y_2) &= (x_2, y_2)\\ (X_3, Y_3) &= (x_3, y_3)\end{aligned}$$

and the inner most triplet

$$\begin{aligned}(X_1, Y_1) &= (x_4, y_4)\\ (X_2, Y_2) &= (x_5, y_5)\\ (X_3, Y_3) &= (x_6, y_6).\end{aligned}$$

We apply the three-point method to these two triplets to obtain two sets of values for the plastochron ratio, divergence angle, and coordinates of the center for the spiral lattice. Table 1 shows the results. We see in the middle two columns that when we have very precise values for the coordinates of the lattice points we can get virtually the same values for the coordinates of C using different triplets of lattice points.

We now want to consider what happens when we add noise to pattern C. We'll perturb each point in pattern C by adding Gaussian noise with a standard deviation of 1. We'll call the resulting configuration "pattern C'" (see figure 1). There are dual interpretations for the meaning of the added noise. First we can think of the added noise as the deviation an individual plant makes from a mathematically ideal pattern. Second we can think of the added noise as experimental errors made in measuring the location of primordia. We shall consider both viewpoints, the first viewpoint will be taken up presently and the second viewpoint will be taken up in section 7.

When we think of pattern C' as the deviation a plant makes from a mathematical ideal we cannot assume the center of the pattern is $(0, 0)$. The perturbations are in random directions which roughly tend to cancel each other out but not perfectly. The effect of the random perturbations is to both distort the ideal pattern and to move it somewhat. So we don't have an

exact position for the center of pattern C' as we did for pattern C.

We can apply the three-point method to the inner and outer triplet of points in pattern C' to try and find the center. The results are shown in the last two columns of table 1. We see that the three-point method only yields approximately the same results with the two triplets. The results are close to $(0, 0)$ as we expect since we hardly perturbed pattern C to get pattern C', but we still don't have an exact position for the center. Without a precise definition for the center of pattern C' we can't even estimate the error of approximation for the three-point method in these examples.

There is another commonly used technique for finding the center that does give us an unambiguous result (Matkowski *et al.*, 1998). This is a center of mass calculation. It is very much like computing the mean of a data set. One treats individual points as having a unit mass and adds together the position vectors of all the points in a data set. The vector sum is then divided by the number of points used in the sum. Let J denote the number of points in a phyllotactic pattern and let the coordinates of the points in the pattern be (x_j, y_j) where $j = 1, \ldots, J$. The center of mass calculation is:

$$\frac{1}{J}\sum_{j=1}^{J}(x_j, y_j)$$

With the three-point method we could only use three points at a time and we got different results using different triplets of points. The center of mass calculation overcomes this problem by making use of the whole data set. It also has the advantage of being much easier to use. However it has a serious drawback. Even with a mathematically perfect spiral lattice the center of mass method will not give accurate results. For example using the center of mass method on pattern C gives $(4.32058, 0.79858)$ which is not even close to $(0, 0)$.

Only in the limit as the number of points used goes to infinity will the center of mass calculation yield the correct position for a perfect spiral lattice. With only a finite number of lattice points there must be some error. The size of the error depends on the number of lattice points used and the divergence angle of the spiral lattice (Matkowski *et al.*, 1998). Since the center of mass method isn't very accurate in mathematically ideal cases it can't be expected to gives us good results for more realistic patterns.

We can combine the three-point method and the center of mass method into a single method. We can use the three-point method on every consecutive triple of points in the pattern to produce a set of points each of which approximates the center of the pattern. We can then find the center of mass for this set of points. This has the advantage of using all of the points and producing an unambiguous result. Furthermore when we apply this combination method to a mathematically ideal case like pattern C it accurately gives us the center. So this combination method has overcome some of the difficulties we ran into using the three-point method or the center of mass method individually. However the most serious difficulty remains. When we apply the combination method to pattern C' we get $(0.15215, -0.39930)$. This appears to be a reasonable approximation for the center of pattern C' but without an exact definition for the center we are unable to estimate the error of approximation. We cannot even claim that the combination method is any more accurate than the three-point method.

Nor is pattern C' a pathological case. Far more distorted phyllotactic patterns are not hard to find. Often in naturally occurring phyllotactic patterns the plastochron ratio is not constant. When the plastochron ratio varies the resulting spiral lattice is no longer an equiangular spiral lattice. A square root spiral lattice is a common occurrence (Williams, 1975). In principal a three point type method can be developed for this type of spiral lattice but its extremely cumbersome. As with the equiangular spiral lattices any deviation in a sample pattern from a perfect square root spiral lattice will just lead to uncertainty about the location of the center.

Not only can the plastochron ratio vary as a plant develops but shoot apices can be ellipsoidal or have even stranger shapes. What is

needed is a definition that does not assume that phyllotactic patterns conform to any mathematical ideal. There is no limit to the number of *ad hoc* methods that can be devised for finding the center of patterns that we believe resemble some mathematically ideal form but without a general definition for the center we can't say which of the many methods is the best.

3. The Minimal Variation Center of a Phyllotactic Pattern

To obtain a general definition for the center of a phyllotactic pattern let's consider how the center is used to study these patterns. The center is the point from which the divergence angles are computed. In well formed phyllotactic patterns the divergence angles are nearly constant. In more distorted specimens there appears to be a greater variability in the divergence angles. It is an open question as to how the variation in the divergence angles arises as we observe increasingly distorted apices. Even though phyllotactic patterns can be strikingly well formed no plant is perfect. To a greater or lesser extent the variation in the divergence angles always plays some role in the developmental process and we'd like to have a better understanding of that role. For example how does the shape of the apex affect the shape of the parastichies?

If we have only a vague idea of where the center is we can only have a vague idea of what the divergence angles are. We could only say that divergence angles tend to become more variable in distorted apices and we would be unable to even address a question like: what affect does the curvature along an ellipsoidal apex have on divergence angles? Finding the center of a phyllotactic pattern will not by itself give us complete answers to questions like this but it is an important step in that direction.

However even in a mathematically ideal pattern we can end up observing variation in the divergence angles if we don't work from the correct point. In a pattern that has been constructed so that the divergence angles are constant an observer can ascertain that the divergence angles are all the same only if they can determine the right point to use to calculate the divergence angles from. If the observer uses a different point they will see some variation in the divergence angles. There are several ways to assess variation in a data set. We shall use the standard deviation to assess the amount of variation in the divergence angles. But regardless of which measure of variation that is used it tends to be the case that the further the point used to calculate the divergence angles is from the point used to construct the pattern the greater the variation that will be observed in the divergence angles.

With a real phyllotactic pattern it will almost never be possible to find a point so that the divergence angles computed relative to that point will be exactly the same between consecutive primordia. As with the mathematically ideal cases the amount of variation that will be observed depends on the point used to calculate the divergence angles. There will be some point inside the pattern that will give the smallest amount of variation. The further the point we use to calculate the divergence angles is from the point that minimizes the variation the larger the variation tends to be. This raises the question of how much of the observed variation is intrinsic to the pattern itself and how much is due to our choice for the center. The best way to provide an objective analysis of this variation is to choose the point in each pattern which minimizes this variation. In mathematically ideal cases the point that does this is of course the point which we already consider to be the center of the spiral lattice (the divergence angles are all the same relative to this point). In real phyllotactic patterns the best we can hope for is to minimize the variation in the divergence angle. Formally:

We define the *minimal variation center* of a two dimensional phyllotactic pattern to be the point inside the pattern that gives the smallest value for the standard deviation of the divergence angles as computed from this point.

The minimal variation center for pattern C' is $(-0.161339, -0.504142)$. Table 2 shows the standard deviation of the divergence angles in pattern C' using the points obtained from the

	Dist.	Std. dev.
outer triplet	0.572	3.33^o
inner triplet	0.304	2.43^o
combination	0.331	2.58^o
min variation	0	2.00^o

Table 2: The rows refer to four points used as the center of pattern C'. The second column shows the distance of the point from the minimal variation center. The third column shows the standard deviation of the divergence angles

three-point and combination methods to calculate the divergence angles from. It also shows the standard deviation we get using the minimal variation center. It is interesting to see how much the standard deviation depends on the point used as the center of pattern C'. No point of pattern C' is any closer to any other point of the pattern than a distance of 15. Yet using a point only a distance 0.572 away from the minimal variation center to calculate the divergence angles from has increased the standard deviation from 2.00 to 3.33. This could give an observer a somewhat exaggerated view of the extent to which the divergence angles in pattern C' deviate from one another.

We have explicitly assumed in the definition of the minimal variation center that the apex is two dimensional. There is also an implicit assumption which is that the divergence angles tend to vary only slightly about their mean value so that it is worthwhile to look for the minimal variation center. We have made no assumptions about the shape of a shoot apex or the type of spiral the parastichies form. Thus the minimal variation center is applicable to a wide variety of phyllotactic patterns.

4. An Algorithm for Finding the Minimal Variation Center

An advantage of having precisely defined our goal is that we can construct algorithms specifically to reach that goal. In this section we will construct one fairly simple algorithm for finding the minimal variation center. This algorithm will be accurate in the sense that in the absence of experimental errors in the data set it will find the minimal variation center of the pattern up to the precision of the computer used to implement the algorithm.

We let (x_{mvc}, y_{mvc}) be the coordinates for the minimal variation center. The algorithm will take an estimate for (x_{mvc}, y_{mvc}) and produce a new point that will be even closer to (x_{mvc}, y_{mvc}). We let (x_0, y_0) be the coordinates for an *estimate* of the minimal variation center's location. By iteration the value of (x_0, y_0) will converge to (x_{mvc}, y_{mvc}).

Let there be J primordia in a sample phyllotactic pattern. Then there will be $J-1$ divergence angles to work with. Let θ_j be the angular position of (x_j, y_j) relative to (x_0, y_0). Let the divergence angle between (x_{j+1}, y_{j+1}) and (x_j, y_j) be $\delta_j = \theta_{j+1} - \theta_j$. The sequence of divergence angles is $\delta_1, \delta_2, \ldots, \delta_{J-1}$.

We seek to minimize the standard deviation, s, of the divergence angles. The value of s is computed from the statistical quantity known as the *sum of squares*, S, according to the formula $s = \sqrt{S/(J-2)}$. Consequently minimizing the value of s is equivalent to minimizing the value of S. It is sufficient, therefore, for the algorithm to just minimize the sum of squares. The sum of squares is defined as

$$S = \sum_{j=1}^{J-1} (\delta_j - \overline{\delta})^2$$

where $\overline{\delta}$ is the mean of the data set $\{\delta_1, \ldots, \delta_{J-1}\}$. Since the value of S depends on $\delta_1, \ldots, \delta_{J-1}$ which in turn depend on (x_0, y_0) we can think of the sum of squares as a function which associates to each point in the plane, (x_0, y_0), the non-negative number S. To indicate the dependence of S on (x_0, y_0) we write $S(x_0, y_0)$. The goal of the algorithm is to find the value for (x_0, y_0) that minimizes $S(x_0, y_0)$.

Computing the gradient of $S(x_0, y_0)$ generally gives us a vector that points in the direction of greatest increase for $S(x_0, y_0)$ while the negative of the gradient points in the direction of greatest decrease for $S(x_0, y_0)$. By following a path that always points in the direction of greatest decrease we generally end up reaching a min-

imum. This is known as the method of gradient descent.

There are several ways to implement gradient descent but one of the simplest will prove quite sufficient for minimizing S. We scale the gradient vector by a small number, ϵ, and then choose a new position for the estimate of the minimal variation center by subtracting the scaled down vector from the old position. Let (X_0, Y_0) denote the new estimate. Our method can be written out as

$$(X_0, Y_0) = (x_0, y_0) - \epsilon \nabla S(x_0, y_0)$$

We then replace the value of (x_0, y_0) with the value of (X_0, Y_0) and do the calculation again. By repeating this calculation over and over the point (x_0, y_0) tends to converge to (x_{mvc}, y_{mvc}). We stop when the magnitude of the gradient vector becomes too small to produce any significant change in the position of (x_0, y_0). Even for a complicated pattern the algorithm can finished in a matter of a few minutes on a modern computer. More information on this algorithm is available in supplementary appendix B[⋆,1]

5. The Algorithm in Operation

In this section we illustrate how the algorithm works by applying it to three configurations.

The first illustration uses pattern C' and it is displayed in figure 2. A sparse configuration like pattern C' shows that it is important that the initial estimate be reasonable. It should be closer to the minimal variation center than any of the points in the pattern. Otherwise gradient descent can lead outside of the configuration and move away from it. From the view of a point far away from the pattern the divergence angles are all close to zero. Consequently the standard deviation of the divergence angles is also close to zero. Once we are too far from the minimal variation center moving even further away can lower the values of the divergence angles and their standard deviation. Therefore the algorithm can lead away from the pattern.

[1] A sample C code that implements this algorithm along with instructions for its use is at http://math.smith.edu/~phyllo/Research/findcenter/findcenter.html

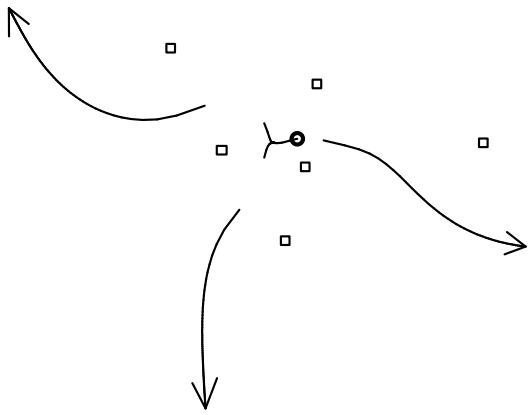

Figure 2: The boxes show the points of pattern C'. Six different initial estimates for the minimal variation center have been used. The circle shows the location of the center of mass which is one of the initial estimates. The six curves show the paths followed by the algorithm with these initial estimates. Three of the initial estimates including the center of mass are close enough to the minimal variation center that the paths go to it. The other three estimates are too far away and the paths go off to infinity.

It is not difficult to choose an initial estimate by inspection but this is not necessary. A useful starting estimate can be obtained from the center of mass method (explained in section 2) so that a computer program only needs to be provided with the coordinates for the position of the points in the configuration. The center of mass for pattern C' is one of the initial estimates for the minimal variation center shown in figure 2.

We now define two mathematically ideal patterns for illustrating this algorithm. We will call these patterns A and B. These are square root lattices and they are very similar, respectively, to the patterns shown in figures $4A$ and $4B$ by Matkowski *et al.* to illustrate their algorithm. As mentioned earlier square root lattices are common in nature (Williams, 1975). We index the points differently here so that the first one corresponds to the oldest primordium of the pattern and the last point corresponds to the newest primordium. The divergence angle is the

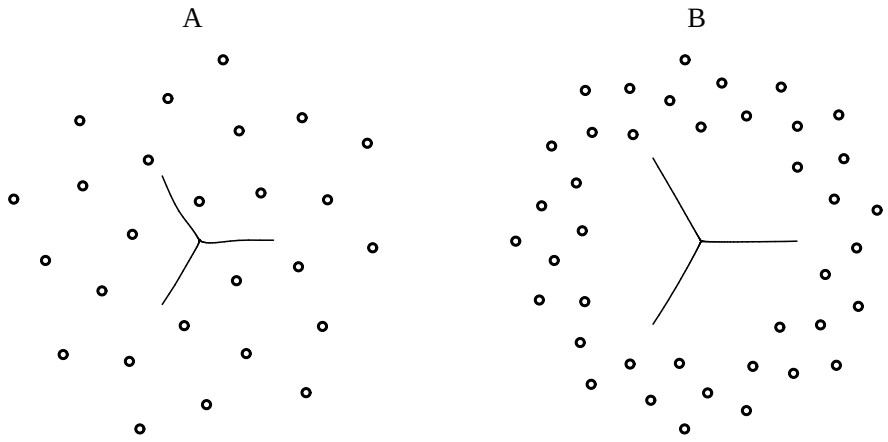

Figure 3: Results of the algorithm with the pattern A and pattern B. The circles denote the positions of the points forming the pattern. The curves show the paths followed by gradient descent to the center from three different initial estimates. The initial estimates lie on the vertices of an equilateral triangle. In pattern A the initial estimates are at a distance of 75 from the center and in pattern B they are at a distance of 160 from the center.

constant $137.5^o = 360^o - 222.5^o$. Pattern A is:

$$\begin{aligned} x_j &= 39.23725\sqrt{27-j}\cos\left(222.5^o(26-j)+90^o\right) \\ y_j &= 39.23725\sqrt{27-j}\sin\left(222.5^o(26-j)+90^o\right) \end{aligned}$$

where $j = 1, \ldots, 26$. Pattern B is:

$$\begin{aligned} x_j &= 40.57925\sqrt{62-j}\cos\left(222.5^o(61-j)+90^o\right) \\ y_j &= 40.57925\sqrt{62-j}\sin\left(222.5^o(61-j)+90^o\right) \end{aligned}$$

where $j = 1, \ldots, 40$. Figure 3 shows patterns A and B and the paths that the algorithm follows from different initial conditions. There are many more points in these two patterns and the starting estimates for the minimal variation center can be much further away from the minimal variation center than in pattern C'. This is particular clear from the illustration for pattern A. For these two mathematically ideal patterns gradient descent went to $(0, 0)$ (up to the precision of the computer). We know that this is the minimal variation center because we have designed the pattern to have constant divergence angles when calculated from $(0, 0)$. This gives zero for the standard deviation of the divergence angles which is the smallest value the standard deviation can have.

It is worth pointing out that the methods employed by Matkowski *et al.* to find the center of these patterns gave approximations that are noticeably different from $(0, 0)$. And the divergence angles obtained with their estimates of the centers fluctuated by several degrees (Matkowski *et al.*, 1998) even though the patterns themselves were mathematically perfect.

To simulate more realistic patterns we have added Gaussian noise with a standard deviation of 5 to A to obtain pattern A' and Gaussian noise with a standard deviation of 10 to pattern B to get pattern B'. Figure 4 shows the perturbed patterns. With this much Gaussian noise the parastichies of the patterns are barely recognizable. They are not unlike what we sometimes see in naturally occurring patterns. The gradient descent algorithm was given the same starting estimates with the perturbed patterns as it was with the unperturbed patterns and it behaved pretty much as it did before. The minimal variation center of pattern A' is $(2.03, -1.15)$. The minimal variation center of pattern B' is $(-2.28, -0.77)$. It is worth noting that for patterns A, B, and C the addition of noise resulted in the minimal variation center moving by less than half the standard deviation of the added noise.

6. The Minimal Variation Center and Uncertainties in the Positions of Primordia

We have defined the minimal variation center of a phyllotactic pattern and we have constructed an algorithm which can accurately find it when there is no uncertainty about the position of the

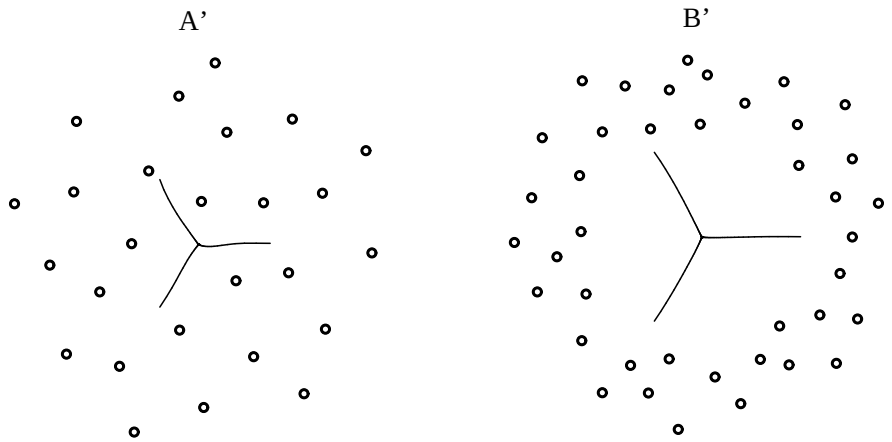

Figure 4: Results of the algorithm with pattern A' and pattern B'. The circles denote the positions of the points forming the pattern. The curves show the paths followed by gradient descent to the center from the same starting points as figure 3

primordia in a phyllotactic pattern. But as was explained in the introduction we can not measure primordia positions precisely. This leads to some uncertainty in the values of the divergence angles. A sequence of divergence angles does not form a set of statistically independent events though. In this section we will see how that fact can work to our advantage. Computing the minimal variation center from less than perfect information on primordia position reduces the effect the uncertainties have on the computation of the divergence angles.

While naturally occurring phyllotactic patterns do resemble spiral lattices we can not assume that if we had precise data on primordia location it would exactly conform to a mathematically ideal configuration or that the divergence angles would all have the same value. We do expect in many cases that the values we compute for the divergence angles will vary only slightly about their mean but we still want to be able to detect the variation in the original sequence as best as we can.

We let $(x_1, y_1), \ldots, (x_J, y_J)$ stand for the location of the primordia in an apex and $\delta_1, \ldots, \delta_{J-1}$ be the divergence angles of the pattern computed using the minimal variation center for the reasons explained in section 3 *i.e.* we don't want the amount of variation in the divergence angles to be an artifact of the point used as the center. We let $(x'_1, y'_1), \ldots, (x'_J, y'_J)$ stand for imprecise measurements of the primordia's positions. The sequence of divergence angles computed from the imprecise data will be denoted by $\delta'_1, \ldots, \delta'_{J-1}$. We will not assume that this sequence of divergence angles was necessarily computed from the minimal variation center of $(x'_1, y'_1), \ldots, (x'_J, y'_J)$.

We want the sequence $\delta'_1, \ldots, \delta'_{J-1}$ to be as close as possible to the original sequence $\delta_1, \ldots, \delta_{J-1}$. One way to measure the distance between two sequences is to form the sum of squares of the differences between corresponding members. To keep the distance the same scale across sequences of different length we divide the sum by $J-1$, the length of the sequence. Finally we take the square root to make the distance the same scale as the differences between corresponding members. This can be written out as

$$\sqrt{\frac{\sum_{j=1}^{J-1}(\delta'_j - \delta_j)^2}{J-1}} \tag{1}$$

Our goal is to make this distance as small as we can without knowledge of the divergence angles $\delta_1, \ldots, \delta_{J-1}$ or the positions $(x_1, y_1), \ldots, (x_J, y_J)$. Without this knowledge we cannot hope to find the exact minimum of (1) but we can at least approximate it.

To approximately minimize (1) we will make use of the fact that the means of the two sequences $\delta_1, \ldots, \delta_{J-1}$ and $\delta'_1, \ldots, \delta'_{J-1}$ are close to each other. The reason for this is as follows. Starting from the first point in the configuration, (x_1, y_1), and going around from one point to the next until we reach the last point (x_J, y_J) we

turn about the minimal variation center by a total amount of $\sum_{j=1}^{J-1} \delta_j$. If instead we start with (x'_1, y'_1) and go around from one point to the next until we reach (x'_J, y'_J) the total amount that we turn will be the sum $\sum_{j=1}^{J-1} \delta'_j$. In either case the total amount that we turn depends only on the angular position of the first and last point - not on the angular position of the intermediate points. The more points there are in the pattern the less it matters that the angular position of (x'_1, y'_1) differs slightly from angular position of (x_1, y_j) and that the angular position of (x'_J, y'_J) differs slightly from the angular position of (x_J, y_J). These slight differences will be small in proportion to the size of the sums $\sum_{j=1}^{J-1} \delta_j$, $\sum_{j=1}^{J-1} \delta'_j$. The mean divergence angles are these sums divided by $J-1$ so the means will be close to each other[2]

Since $\overline{\delta} \approx \overline{\delta}'$ we get

$$\frac{\sum_{j=1}^{J-1}(\delta'_j - \overline{\delta})^2}{J-1} \approx \frac{\sum_{j=1}^{J-1}(\delta'_j - \overline{\delta}')^2}{J-1} \qquad (2)$$

Now since we use the minimal variation center to prevent undue variation in the sequence $\delta_1, \ldots, \delta_{J-1}$ we keep the values of δ_j close to $\overline{\delta}$. This gives us the approximation

$$\frac{\sum_{j=1}^{J-1}(\delta'_j - \delta_j)^2}{J-1} \approx \frac{\sum_{j=1}^{J-1}(\delta'_j - \overline{\delta})^2}{J-1} \qquad (3)$$

If the divergence angles $\delta_1, \ldots, \delta_{J-1}$ are all the same then (3) becomes a strict equality. As the standard deviation of $\delta_1, \ldots, \delta_{J-1}$ rises above zero the left and right hand sides of (3) can move apart. So long as the standard deviation is small enough the right hand side is a good approximation of the left hand side.

We can combine expressions (2) and (3) to get

$$\frac{\sum_{j=1}^{J-1}(\delta'_j - \delta_j)^2}{J-1} \approx \frac{\sum_{j=1}^{J-1}(\delta'_j - \overline{\delta}')^2}{J-1} \qquad (4)$$

[2]The mean divergence angle is closely related to the concept of the rotation number of an orientation preserving diffeomorphism of a circle to itself. The argument presented above for the close proximity of the mean divergence angles is a variation of a step in the proof of the theorem that the rotation numbers of C^0-close orientation preserving diffeomorphism of a circle have approximately the same value. For a concise presentation of a proof of this theorem see (Devaney, 1989).

The left hand side is the expression under the radical in (1) which we want to minimize. The right hand side can be computed entirely from $(x'_1, y'_1), \ldots, (x'_J, y'_J)$. (An estimate for the error of approximation in expression (4) is in supplementary appendix C*. As was explained in section 4 using the minimal variation center to compute the divergence angles $\delta_1, \ldots, \delta_{J-1}$ minimizes the numerator of the right hand side of (4). Thus finding the minimal variation center of the points $(x'_1, y'_1), \ldots, (x'_J, y'_J)$ provides us with a way of approximately minimizing (1). We can use it under those circumstances where both (2) and (3) are good approximations *i.e.* when there are a large number of divergence angles and the divergence angles vary only slightly about their mean.

7. Finding Divergence Angles: Four Examples

We now provide four demonstrations of the usefulness of the minimal variation center for recovering the underlying sequence of divergence angles of a phyllotactic pattern from imprecise data. In this section we will now interpret noise added to a pattern as experimental errors made in the measurement of primordia positions. We will compute approximate values for the divergence angles of the original patterns using only the noisy data. The divergence angles will be computed using both the minimal variation center and the center of mass. We will see that the minimal variation center does a better job of finding the divergence angles.

We begin with patterns A and B which have over two dozen points each and whose divergence angles are a constant 137.5^o. These two patterns are too perfect to be natural. They represent ideal cases where we expect to get good results for the divergence angles because approximation (3) in section 6 is an equality for these cases. We add Gaussian noise with a standard deviation of 2 to pattern A to get pattern A'' and we add Gaussian noise with a standard deviation of 4 to pattern B to get pattern B''.

The divergence angles are shown in figures 5 and 6. The original sequences are constant and

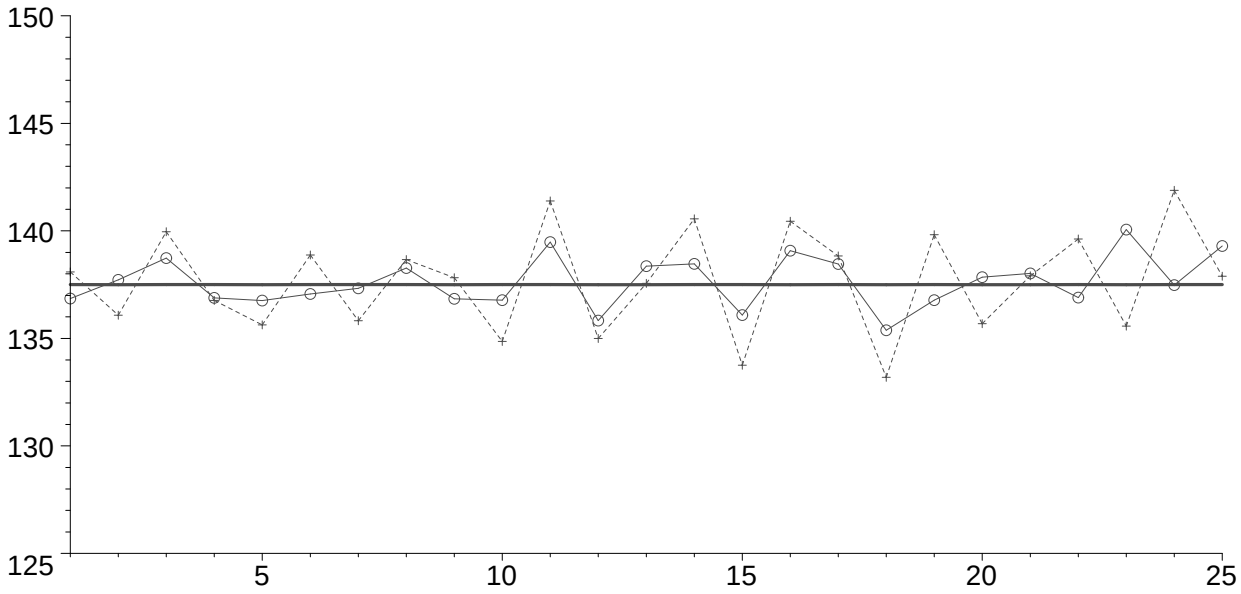

Figure 5: The thick line marks 137.5^o - the value for every divergence angle in pattern A. The thin solid line passing through the open circles shows the sequence of divergence angles in pattern A'' using the minimal variation center to compute the angles. The dotted line passing through the crosses shows the sequence of divergence angles in pattern A'' using the center of mass to compute the angles.

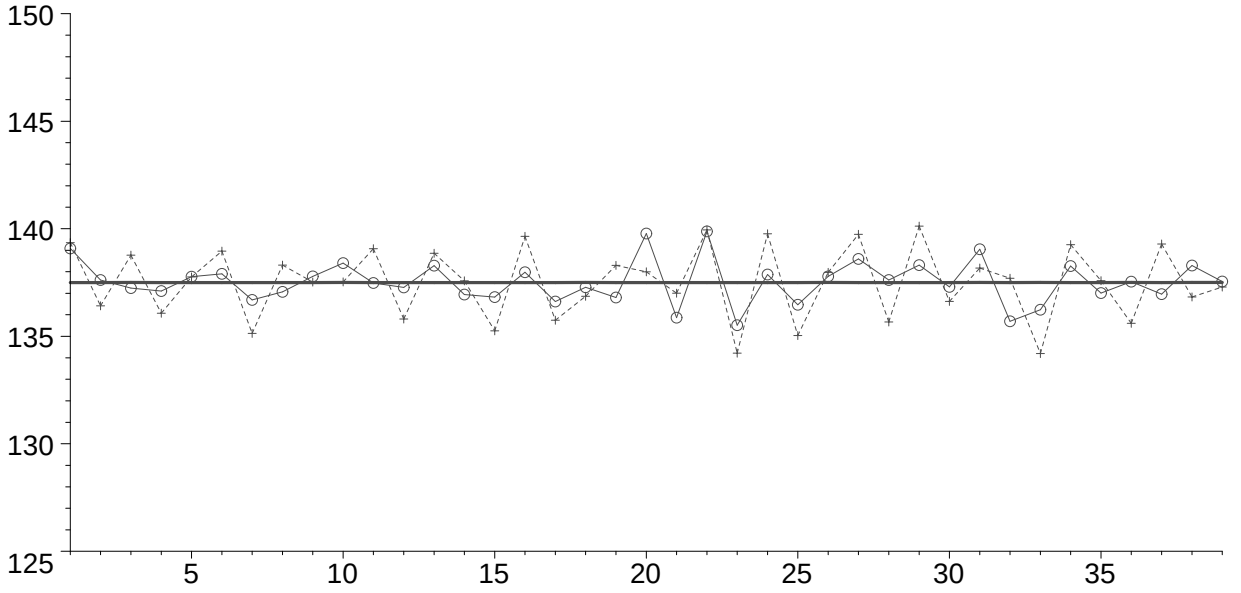

Figure 6: The thick line marks 137.5^o - the value for every divergence angle in pattern B. The thin solid line passing through the open circles shows the sequence of divergence angles in pattern B'' using the minimal variation center to compute the angles. The dotted line passing through the crosses shows the sequence of divergence angles in pattern B'' using the center of mass to compute the angles.

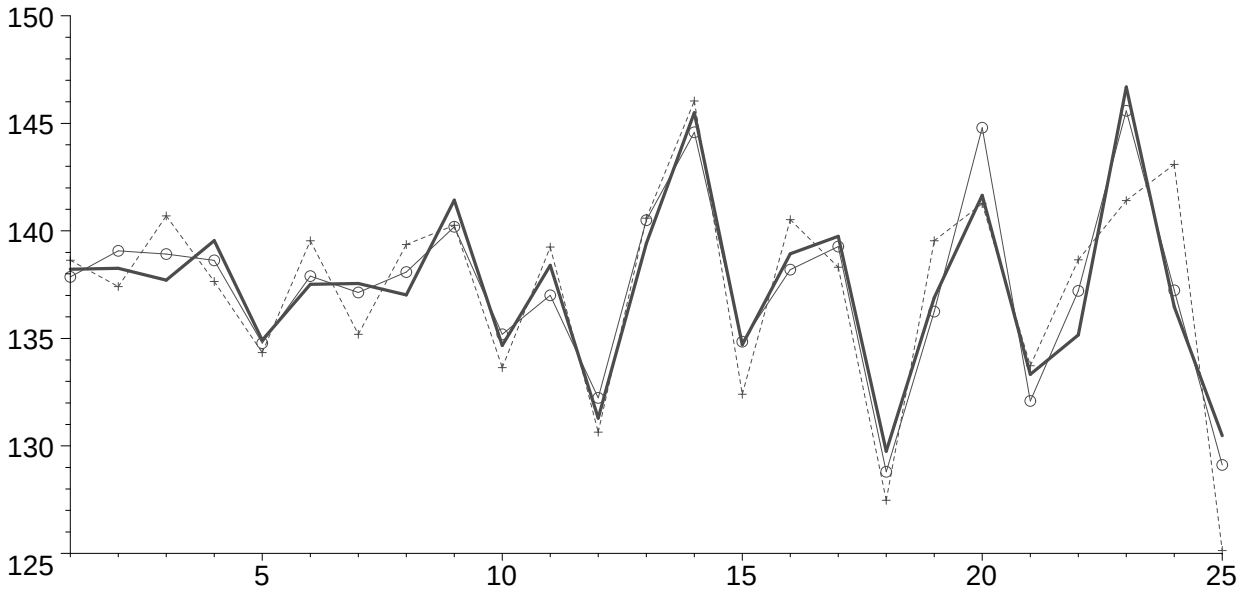

Figure 7: The thick line indicates the sequence of divergence angles in pattern A' using the minimal variation center to compute the angles. The thin solid line passing through the open circles shows the sequence of divergence angles in pattern A''' using the minimal variation center to compute the angles. The dotted line passing through the crosses shows the sequence of divergence angles in pattern A''' using the center of mass to compute the angles.

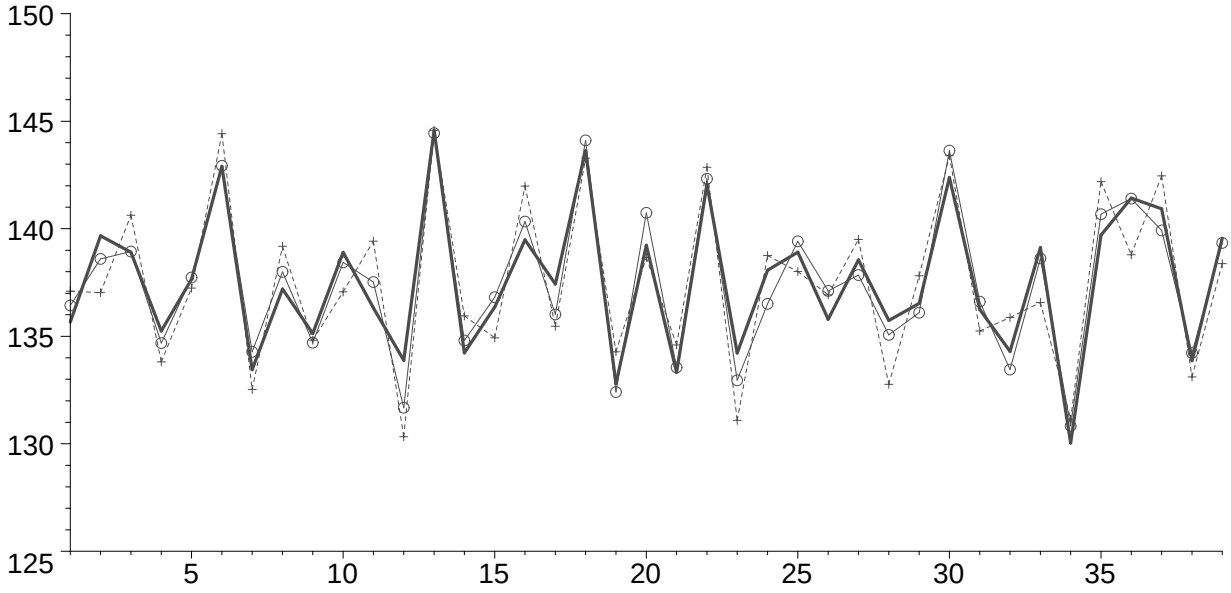

Figure 8: The thick line indicates the sequence of divergence angles in pattern B' using the minimal variation center to compute the angles. The thin solid line passing through the open circles shows the sequence of divergence angles in pattern B''' using the minimal variation center to compute the angles. The dotted line passing through the crosses shows the sequence of divergence angles in pattern B''' using the center of mass to compute the angles.

the sequences obtained from the perturbed patterns using the minimal variation center is closer to being level than the sequences obtained using the center of mass. We can not expect to completely overcome the effects of the noise that has been added to patterns A and B. We see in figures 5 and 6 that some of the divergence angles deviate from 137.5^o by a few degrees regardless of whether we use the minimal variation center or the center of mass. For the vast majority of divergence angles, though, the value obtained using the minimal variation center is closer to original value than the value obtained using the center of mass. So we have, at least, reduced the effect of the noise by using the minimal variation center.

The next two examples are based on patterns A' and B'. The divergence angles in patterns A' and B' vary by several degrees. We interpret these configurations as the location of primordia in a pair of phyllotactic patterns that do not conform to a mathematical ideal. We continue to interpret the noise in patterns A' and B' as a natural deviation plants make from a mathematical ideal form. We add more noise to patterns A' and B' which we interpret as experimental errors in the measurement of primordia position. We add Gaussian noise with a standard deviation of 2 to pattern A' to get pattern A''' and we add Gaussian noise with a standard deviation of 4 to pattern B' to get pattern B'''[3]. The divergence angles are shown in figures 7 and 8.

We can see in figures 7 and 8 that the sequences of divergence angles in patterns A''' and B''' computed with the minimal variation center does follow the original sequence more closely than the sequences computed using the center of mass. Not every divergence angle computed with the minimal variation center of pattern A''' is closer to its corresponding value in pattern A' but there clearly is an overall tendency for the corresponding values to be closer when the minimal variation center is used to compute the divergence angles. The same things holds for pattern B'''.

[3] Data files for patterns A,A',A'',A''',B,B',B'',B''',C, and C' are at http://math.smith.edu/~phyllo/Research/findcenter/findcenter.html

Distance	Min. Var.	CM
Pattern A''	1.17^o	2.33^o
Pattern B''	1.14^o	2.60^o
Pattern A'''	0.98^o	1.63^o
Pattern B'''	0.86^o	1.76^o

Table 3: Each of the four rows refers to a pattern that has been perturbed to simulate the effect of experimental errors (see text for a description of each pattern). The table shows the distance between the sequence of divergence angles in the perturbed pattern and the sequence of divergence angles in the corresponding unperturbed pattern. In the second column the minimal variation center has been used to compute the divergence angles in the perturbed pattern. In the third column the center of mass has been used to compute the divergence angles in the perturbed pattern.

The distances (as defined by (1) in section 6) between the original sequences and the sequences obtained from the perturbed patterns are shown in table 3. For each of the patterns the table clearly shows that the minimal variation center provides us with the sequence of divergence angles which is closer to the original sequence.

We can expect similar results with naturally occurring phyllotactic patterns whose divergence angles deviate less about their mean values than the divergence angles of patterns A' and B' do. We can see in figure 4 that patterns A' and B' deviate quite noticeably from a mathematically ideal form. They are not unrealistic but more well formed patterns are fairly common in nature. The minimal variation center can be a useful tool to uncover systematic variations in the divergence angles which may arise in capitula that are slightly imperfect.

8. Phyllotaxis in Three Dimensions

Although the shape of capitula tend to be well approximated by a flat disk most apices are dome or conical shaped. In these cases the primordia form a three dimensional configuration. The addition of an extra dimension means that the center of the pattern in space is no longer merely

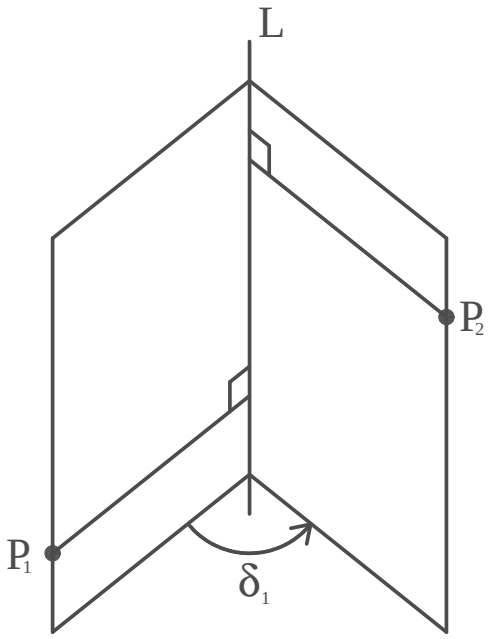

Figure 9: Given two points, P_1, P_2 and a line L there is a unique plane containing L and P_1 and a unique plane containing L and P_2. We take the dihedral angle between the planes as the angle between P_1 and P_2 relative to L. This angle is labeled δ_1.

a point but a curve. This curve is known as the *axis* of the shoot. We do not want the axis to be curved any more than necessary. Mathematically speaking we want the curvature at each point of the axis to remain within a certain bound and for the integral curvature to be small. In this paper we will focus mainly on the case where the axis is straight (*i.e.* when the curvature is zero everywhere).

The divergence angle between consecutive primordia needs to be calculated relative to the axis. Computing divergence angles is much easier when the curve is a straight line where we can make use of the dihedral angle between two planes that meet at the axis (see figure 9). When the axis is not straight we need to generalize the concept of a dihedral angle. To do this for an axis that is sufficiently smooth we can make use of the Serret-Frenet frame of the curve but we leave this to be a topic for a future paper.

As in the planar cases the divergence angles in many three dimensional phyllotactic patterns tend to vary only slightly about some particular value (*e.g.* 137.5^o). Some phyllotactic patterns show greater variation in their divergence angles than others. Computing these divergence angles requires a good estimate for the location of the axis. Like in the planar case we don't want the variation in the divergence angles to be an artifact of the choice for the shoot's axis. We would like to choose a curve that minimizes the variation in the divergence angles. However for any finite configuration of points we can find a sufficiently winding curve so that the divergence angles computed relative to this curve will all be zero. Such a curve would be a poor choice for the axis of most any configuration. We need to strike a balance between the amount of curvature in the axis and the amount of variation in the divergence angles. For now we will only consider axis that are straight. Formally

We provisionally define the *minimal variation axis* of a three dimensional phyllotactic pattern to be the line passing through the pattern that gives the smallest value for the standard deviation of the divergence angles as computed from this line.

With this definition for the axis of a three dimensional phyllotactic pattern we can construct an algorithm to find it. The algorithm will be based on gradient descent. We need to establishing a coordinate system to work in. First we have to decide where the origin is going to be. The location of the origin is only a matter of convenience and a convenient spot is near the tip of the shoot. This is also a conventional choice in making measurements for the location of primordia of three dimensional patterns. It would be most convenient if the minimal variation axis were to pass through the origin but that is too much to expect before we have found it. We have to be content with putting the origin close to where the minimal variation axis meets the tip of the apex.

We will choose our initial estimate for the minimal variation axis to be the vertical coordinate axis which we will call the w-axis. The positive direction will point up. The remaining two coordinate axes will be called the u-axis and

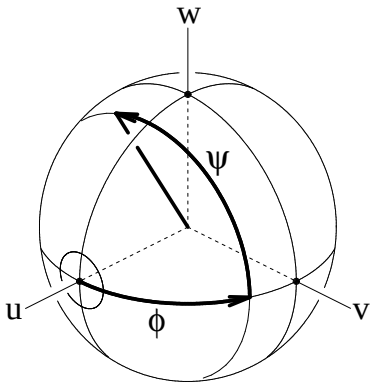

Figure 10: A unit vector is shown as the thick straight line. Its position is given in terms of (ϕ, ψ). These two angles are shown as thick arcs. The u-axis is the "pole", ϕ gives the angle between the vector and the positive u-axis, and ψ gives the angle of rotation about the u-axis from the horizontal direction to the vector.

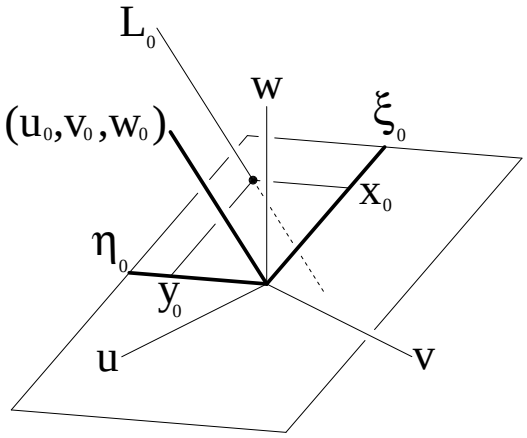

Figure 11: The vectors ξ_0, η_0 form an orthonormal basis for the plane which is perpendicular to the line L_0 and which passes through the origin. The point where L_0 passes through this plane is $x_0\xi_0 + y_0\eta_0$.

v-axis. We place them so that the u, v, w-axes form a right handed orthogonal coordinate system. As we iterate the algorithm our estimate for the location of the minimal variation axis will be updated but we will keep the coordinate system fixed.

To specify the location of a line we need a vector pointing in the direction of the line and the location of some point that the line passes through. It is convenient to use unit vectors to specify the direction of a line. The set of all unit vectors forms a sphere of radius 1 about the origin. We can use spherical coordinates to specify a unit vector on this sphere (see figure 10). Each pair of angles (ϕ, ψ) will specify the unit vector

$$(\cos(\phi), \sin(\phi)\cos(\psi), \sin(\phi)\sin(\psi))$$

This is slightly different from the usual form for spherical coordinates. We choose this form so that the coordinate singularities[4] are at $(\pm 1, 0, 0)$. These are perpendicular to the estimated direction of the minimal variation axis so that the algorithm is not likely to venture near them.

We let (ϕ_m, ψ_m) specify the direction of the minimal variation axis and (ϕ_0, ψ_0) specify an estimate for the direction of the minimal variation axis. The initial estimate for the direction of the minimal variation axis is $(90^o, 90^o)$ but as we iterate the algorithm we will update the values for (ϕ_0, ψ_0) so that they become closer to (ϕ_m, ψ_m). The corresponding unit vectors are

$$(u_m, v_m, w_m) = (\cos(\phi_m), \sin(\phi_m)\cos(\psi_m), \sin(\phi_m)\sin(\psi_m))$$

$$(u_0, v_0, w_0) = (\cos(\phi_0), \sin(\phi_0)\cos(\psi_0), \sin(\phi_0)\sin(\psi_0))$$

The point in the line that we will use to specify it is where it meets the plane which passes through the origin and which is perpendicular to the line. The vectors

$$\overrightarrow{\xi}_m = (-\sin(\phi_m), \cos(\phi_m)\cos(\psi_m), \cos(\phi_m)\sin(\psi_m))$$
$$\overrightarrow{\eta}_m = (0, -\sin(\psi_m), \cos(\psi_m))$$

form an orthonormal basis for the plane which passes through the origin and which is perpendicular to (u_m, v_m, w_m). Wherever this plane meets the minimal variation axis there is a unique pair of numbers (x_m, y_m) such that the intersection point can be expressed as $x_m \overrightarrow{\xi}_m + y_m \overrightarrow{\eta}_m$. The minimal variation axis is the set of points

$$L_m = \{(u_m, v_m, w_m)t + x_m \overrightarrow{\xi}_m + y_m \overrightarrow{\eta}_m : t \in \mathbb{R}\}$$

The minimal variation axis is completely specified by the numbers $(\phi_m, \psi_m, x_m, y_m)$.

[4] Coordinate singularities are like the north and south poles where the Earth's "lines" of longitude meet

Similarly the vectors

$$\begin{aligned}\overrightarrow{\xi}_0 &= (-\sin(\phi_0), \cos(\phi_0)\cos(\psi_0), \cos(\phi_0)\sin(\psi_0)\\ \overrightarrow{\eta}_0 &= (0, -\sin(\psi_0), \cos(\psi_0))\end{aligned}$$

form an orthonormal basis for the plane through the origin that is perpendicular to (u_0, v_0, w_0). There is a unique pair of numbers (x_0, y_0) such that this plane meets our estimate for the minimal variation axis at $x_0\overrightarrow{\xi}_0 + y_0\overrightarrow{\eta}_0$ (see figure 11). The estimate for the minimal variation axis is the set of points

$$L_0 = \{(u_0, v_0, w_0)t + x_0\overrightarrow{\xi}_0 + y_0\overrightarrow{\eta}_0 : t \in \mathbb{R}\}$$

This line is completely specified by the numbers $(\phi_0, \psi_0, x_0, y_0)$.

The algorithm we are constructing will take the estimate $(\phi_0, \psi_0, x_0, y_0)$ and produce an new estimate that will be closer to $(\phi_m, \psi_m, x_m, y_m)$. We do this by applying gradient descent to the sum of squares, S, of the divergence angles computed relative to the line L_0.

Assume the positions of the sequence of points $P_1, \ldots, P_J$ of the three dimensional configuration have been measured and recorded as (u_1, v_1, w_1), $\ldots, (u_J, v_J, w_J)$ respectively. To compute the divergence angles relative to L_0 from (u_1, v_1, w_1), $\ldots$, (u_J, v_J, w_J) we can orthogonally project the spatial configuration into a plane perpendicular to L_0 (see figure 12). The computation of the divergence angles in a spatial configuration is then reduced to the computation of divergence angles of a planar configuration.

Let us denote the projection of (u_j, v_j, w_j) into the plane by (x_j, y_j). Since $\overrightarrow{\xi}_0, \overrightarrow{\eta}_0$ form an orthonormal basis for the plane containing the origin and perpendicular to L_0 we get explicit expressions for x_j and y_j by using the dot product.

$$\begin{aligned}x_j = (u_j, v_j, w_j) \bullet \overrightarrow{\xi}_0 =\\ -u_j\sin(\phi_0) + \cos(\phi_0)(v_j\cos(\psi_0) + w_j\sin(\psi_0))\end{aligned}$$

$$y_j = (u_j, v_j, w_j) \bullet \overrightarrow{\eta}_0 = -v_j\sin(\psi_0) + w_j\cos(\psi_0)$$

The computation of the divergence angles $\delta_1, \ldots, \delta_{J-1}$ of $(x_1, y_1), \ldots, (x_J, y_J)$ relative to (x_0, y_0) proceeds just as it did in the planar case. From

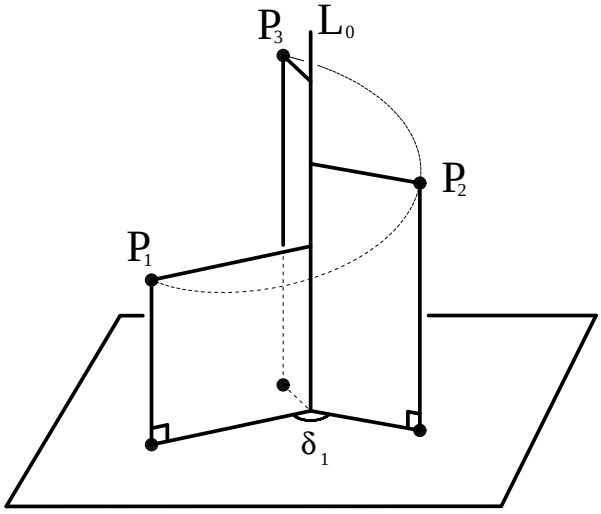

Figure 12: The angle between points relative to L_0 is preserved when we orthogonally project the points into any plane that is perpendicular to L_0. (The plane in this figure is not the one that passes through the origin.)

$\delta_1, \ldots, \delta_{J-1}$ we can compute

$$S = \sum_{j=1}^{J-1}(\delta_j - \overline{\delta})^2$$

S is now a function of $(\phi_0, \psi_0, x_0, y_0)$. Gradient descent can be expressed as

$$(\Phi_0, \Psi_0, X_0, Y_0)$$

$$= (\phi_0, \psi_0, x_0, y_0) - \epsilon\nabla S(\phi_0, \psi_0, x_0, y_0)$$

where ϵ is a small number that scales down the length of the gradient vector. We then replace $(\phi_0, \psi_0, x_0, y_0)$ with $(\Phi_0, \Psi_0, X_0, Y_0)$ and repeat. For a detailed computation of the gradient vector see supplementary appendix $D^{\star,1}$

With the minimal variation axis we can recover the sequence of divergence angles in three dimensional phyllotactic patterns. Experimental errors in the measurement of primordia positions will limit the precision with which we can recover the angles. The arguments of section 6 (and supplementary appendix $C^\star$) require very little modification for three dimensional patterns. So long as the standard deviations are small and the number of primordia is large approximation

(4) of section 6 remains valid and using the minimal variation axis to compute the divergence angles reduces the impact of experimental errors in three dimensions just as the minimal variation center reduces their impact in two dimensions. The possibility exists that the impact of these experimental errors could be further reduced by using an appropriately chosen curve instead of a line to compute the divergence angles from.

A program which implements this algorithm can complete the calculations in a matter of minutes on a modern desktop computer[5]

9. Summary

The field of phyllotaxis has been challenged by the diversity of shapes that shoot apices can have. This paper has introduced the concept of the minimal variation center to help deal with this diversity. The minimal variation center provides us with an objective way to compute divergence angles in capitula whose primordia do not conform perfectly to a spiral lattice. It also helps to mitigate the effect experimental errors in the measurement of the primordia positions have on the computed values of the divergence angles. This helps lay the groundwork to objectively compare theory against experiment for a more general class of phyllotactic patterns[6].

Acknowledgment

I wish to thank Roger Meicenheimer for many useful discussions about bridging the gap between theory and experiment. I'd also like to thank the Department of Mathematics & Statistics of Miami University and the Mathematics Department of Smith College for the use of their computers.

REFERENCES

Atela, P., Golé C., & Hotton S. (2002), A Dynamical System for Plant Pattern Formation: A Rigorous Analysis, *J. Nonlinear Sci.* **12** (6) pp. 641-676.

Bravais, L. & Bravais, A. (1837), Essai sur la disposition des feuilles curvisériées. *Ann. Sci. Nat.* **7** pp. 42-110, Essai sur la disposition symmétrique des inflorescences. *Ann. Sci. Nat.* **7** pp. 193-221 and 291-348; *Ann. Sci. Nat.* **8** pp. 11-42.

Devaney, R. (1989) *An Introduction Chaotic Dynamical Systems* 2nd. ed., Boston: Addison-Wesley Pub. Co.

Douady S. & Couder Y. (1996), Phyllotaxis as a Self Organizing Iterative Process, Part I, *J. Theor. Biol.* **178** pp. 255-274.

Dumais, J. and Kwiatkowska, D. (2002), Analysis of surface growth in shoot apices, *Plant Journal* **31** pp. 229-241.

Hernandez, L.F., Havelange, A., Bernier, G. & Green, P.B. (1991), Growth behavior of single epidermal cells during flower formation: Sequential scanning electron micrographs provide kinematic patterns for Anagallis, *Planta* **185** pp. 139-147.

Hill, J.P. (2001) Meristem development at the sporophyll pinna apex in *Ceratopteris richardii*, *Int. J. Plant Sci.* **162** pp. 235-247.

Hofmeister W. (1868), Allgemeine Morphologie der Gewachse, in *Handbuch der Physiologischen Botanik*, **1** Engelmann, Leipzig pp. 405-664.

Maksymowych R. & Erickson R.O. (1977), Phyllotactic Change Induced by Gibberellic Acid in *Xanthium* Shoot Apices, *Amer. J. Bot.* **64** pp. 33-44.

Matkowski A., Karwowski R. & Zagórska-Marek B. (1998), Two Algorithms of Determining the Middle Point of the Shoot Apex by Surrounding Organ Primordia Positions and their Usage for Computer Measurements of Divergence Angles, *Acta Soc. Bot. Pol.* **67** (2) pp 151-159.

Meicenheimer R.D. (1986), Role of Parenchyma in Linum Usitatissimum Leaf Trace Pattern, *Amer. J. Bot.* **12** pp. 1649-1664.

Sattler, R. (1973) *Organogenesis of flowers; a photographic text-atlas*, Toronto & Buffalo: University of Toronto Press

Williams M.H. & Green P.B. (1988) Sequential scanning electron microscopy of a growing plant

[5] A sample C code that implements this algorithm along with instructions for its use is at http://math.smith.edu/~phyllo/Research/findcenter/findcenter.html

[6] Supplementary appendices are available at doi:00000000000000000000000000000.

meristem. *Protoplasma* **147** pp. 77-79

Williams R.F. (1975), *The Shoot Apex and Leaf Growth*, Cambridge: Cambridge University Press.

Appendix A

In this appendix we derive formulas for the parameters of an equiangular spiral lattice from three consecutive lattice points. Let P_1, P_2, P_3 be three consecutive lattice points where P_1 is the outermost and P_3 is the innermost lattice point. Let C be the center of the spiral lattice (see figure 13). Recall that the coordinate of P_1, P_2, P_3 are $(X_1, Y_1), (X_2, Y_2), (X_3, Y_3)$ respectively and the coordinates of C are (x_c, y_c).

Figure 13 shows that value of a equals the length of $\overline{P_1P_2}$ divided by the length of $\overline{P_2P_3}$. In coordinates this is

$$a = \sqrt{\frac{(X_2 - X_1)^2 + (Y_2 - Y_1)^2}{(X_3 - X_2)^2 + (Y_3 - Y_2)^2}}$$

To obtain δ we extend $\overline{P_1P_2}$ to $\overline{P_1A}$. Figure 14 shows that δ equals $\angle AP_2P_3$. The angle that $\overline{P_1A}$ makes with a horizontal line is the same as the angle $\overline{P_1P_2}$ makes with a horizontal line. This angle is given by $\text{atan2}(Y_2 - Y_1, X_2 - X_1)$. The angle that $\overline{P_2P_3}$ makes with a horizontal line is $\text{atan2}(Y_3 - Y_2, X_3 - X_2)$. The difference between these two is δ:

$$\begin{aligned}\delta = &\text{atan2}(Y_3 - Y_2, X_3 - X_2)\\ &-\text{atan2}(Y_2 - Y_1, X_2 - X_1)\end{aligned}$$

The atan2 function is explained in appendix B.

We can apply the law of cosines to $\triangle P_2CP_3$ to obtain the value of R. Looking at figure 13 we see the law of cosines in this case gives:

$$Q^2 = R^2 + (aR)^2 - 2(R)(aR)\cos(\delta)$$

We know $Q^2 = (X_3 - X_2)^2 + (Y_3 - Y_2)^2$. Solving for R gives:

$$R = \sqrt{\frac{(X_3 - X_2)^2 + (Y_3 - Y_2)^2}{1 + a^2 - 2a\cos(\delta)}}$$

Point C lies at distance R from P_3 and it lies at distance aR from P_2 (see figure 15). Or in other words it must be one of the places where the circle with radius R about P_3 intersects the circle with radius aR about P_2. The equations for these two circles are

$$\begin{aligned}(aR)^2 &= (x - X_2)^2 + (y - Y_2)^2\\ R^2 &= (x - X_3)^2 + (y - Y_3)^2.\end{aligned}$$

The coordinates for the intersection points of these two circles are given by those values of (x, y) which satisfy both of these equations. Solving these two equations is tedious. We only provide the solution here. First define the following four quantities:

$$x_\pm = \frac{(a\cos(\delta) - 1)(X_3 - X_2) \pm a\sin(\delta)(Y_3 - Y_2)}{1 + a^2 - 2a\cos(\delta)}$$

$$y_\pm = \frac{(a\cos(\delta) - 1)(Y_3 - Y_2) \pm a\sin(\delta)(X_3 - X_2)}{1 + a^2 - 2a\cos(\delta)}$$

The intersection points are

$$\begin{aligned}&((x_+) + X_3, (y_-) + Y_3)\\ &((x_-) + X_3, (y_+) + Y_3)\end{aligned}$$

Point C must be one of these two points. These formulas for the center are similar to the ones presented in (Meicenheimer, 1986). With the

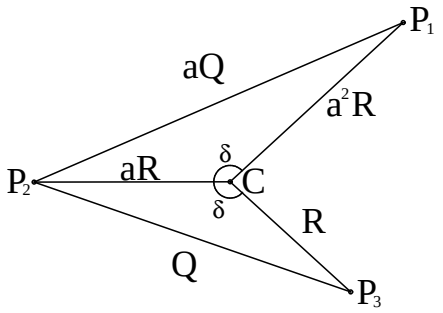

Figure 13: The length of $\overline{P_2C}$ is a times the length of $\overline{P_3C}$. The length of $\overline{P_3C}$ is denoted by R in the figure. The length of $\overline{P_1C}$ is a times the length of $\overline{P_2C}$. Since $\delta = \angle P_1CP_2 = \angle P_2CP_3$ the triangles $\triangle P_1CP_2$ and $\triangle P_2CP_3$ are similar. Therefore the length of $\overline{P_1P_2}$ is a times the length of $\overline{P_2P_3}$. The length of $\overline{P_2P_3}$ is denoted by Q in the figure.

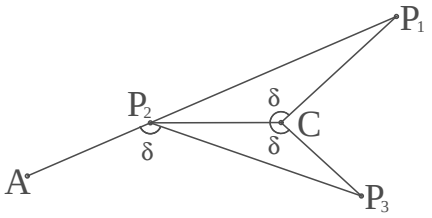

Figure 14: The sum of the angles in $\triangle P_1CP_2$ is 180^o and the points P_1, P_2, A are collinear. This gives us the equation $\angle P_1P_2C + \angle CP_1P_2 + \angle P_1CP_2 = \angle P_1P_2C + \angle CP_2P_3 + \angle AP_2P_3$. Since $\angle P_1P_2C$ appears on both sides we can cancel those terms. And since $\triangle P_1CP_2$ is similar to $\triangle P_2CP_3$ the angles $\angle CP_1P_2$ and $\angle CP_2P_3$ are equal. We can cancel them from the equation as well. This leaves $\angle P_1CP_2 = \angle AP_2P_3$.

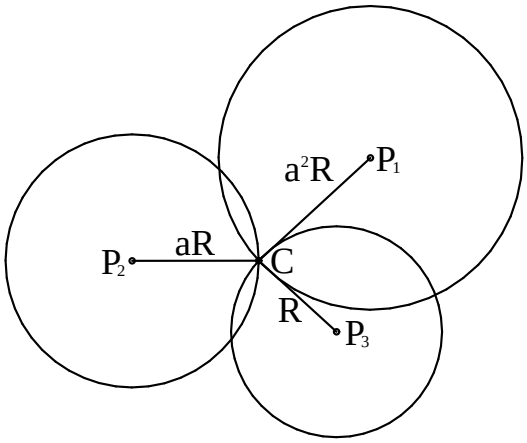

Figure 15: The point C lies on a circle of radius R about P_3. It also lies on a circle of radius aR about P_2 and on a circle of radius a^2R about P_1. The location of C can be determined from the fact that these three circles only intersect simultaneously in a single point.

formulas here it is easier to see how the number of intersection points between the two circles depends on the divergence angle. Except when $\delta = 0^o$ or $\delta = 180^o$ there are two distinct intersection points. When $\delta = 0^o$ or $\delta = 180^o$ the circles intersect in a single point which is C so no choice has to be made.

For the case $\delta \neq 0^o$ and $\delta \neq 180^o$ a choice needs to be made for C. Since C must lie on the circle with radius a^2R about P_1 a rigorous way to determine which of these two intersection points is actually C is to plug each into the equation:

$$(a^2R)^2 = (x - X_1)^2 + (y - Y_1)^2$$

The correct choice for (x_c, y_c) will satisfy this equation while the incorrect choice will not.

Appendix B

The tangent function has a period of 180^o *i.e.* $\tan(\theta + 180^o) = \tan(\theta)$. Consequently the inverse of the tangent function is not uniquely defined. However if we restrict the domain of tan to the interval between -90^o and 90^o it becomes a continuous one to one map onto the real line. This makes it convenient to restrict the range of the inverse function to the interval between -90^o and 90^o. This gives a continuous function that is one to one on the whole real line. This inverse is called *arctan*.

Even though arctan is a convenient function it cannot give us the angular coordinate for some points in plane. For example consider the points $(1, 1)$ and $(-1, -1)$. They are collinear with the origin and the slope of this line is 1. We can substitute this slope into the arctan function to get the angular coordinate of $(1, 1)$ (*i.e.* the angle that the ray starting at the origin and passing through $(1, 1)$ makes with the positive x-axis). This angle is $45^o = \arctan(1)$. However the angular coordinate of $(-1, -1)$ is -135^o (or 225^o) which is outside of the range of arctan.

One way to avoid this problem is to define a function which makes use of both the horizontal and vertical coordinates of the point. That is the purpose of the atan2 function. Its range is the interval between -180^o and 180^o along with the value 180^o. The atan2 function can be defined

in terms of arctan as follows:

$$\begin{aligned}
\text{atan2}(y,x) &= \arctan(y/x) && \text{if } x > 0 \\
\text{atan2}(y,x) &= \arctan(y/x) + 180^o && \text{if } x < 0,\ y \geq 0 \\
\text{atan2}(y,x) &= \arctan(y/x) - 180^o && \text{if } x < 0,\ y < 0 \\
\text{atan2}(y,0) &= 90^o && \text{if } y > 0 \\
\text{atan2}(y,0) &= -90^o && \text{if } y < 0
\end{aligned}$$

atan2 is left undefined for the point $(0,0)$. Note that it is conventional to put the y coordinate before the x coordinate in atan2.

An analysis of a phyllotactic pattern in the early stages of development begins with measurements for the position of the primordia. Let the primordia be labeled in ontological order so that oldest one is labeled "1", the second oldest is labeled "2", and so on up to the newest one which is labeled "J". Let the horizontal and vertical coordinates measured for the j^{th} primordium be (x_j, y_j).

If the origin of the coordinate system is used as the center of the pattern then the angular coordinate of (x_j, y_j) would simply be $\text{atan2}(y_j, x_j)$. However we want the angle that a ray starting at our initial estimate for the center, (x_0, y_0), and passing through (x_j, y_j) makes with a horizontal ray starting at (x_0, y_0). To do this we need to take the vector difference between (x_j, y_j) and (x_0, y_0) before using the atan2 function. In a sense we are translating our coordinate system so that (x_0, y_0) becomes the origin and $(x_j - x_0, y_j - y_0)$ are the coordinates for the j^{th} primordium. We denote the angular coordinate of the j^{th} primordium by θ_j. It is given by

$$\theta_j = \text{atan2}(y_j - y_0, x_j - x_0).$$

We denote the divergence angle between the j^{th} and $j+1^{th}$ primordium by δ_j. There are $J-1$ divergence angles altogether. They are given by

$$\delta_j = \theta_{j+1} - \theta_j.$$

The formula for gradient descent is

$$(X_0, Y_0) = (x_0, y_0) - \epsilon \left(\frac{\partial S}{\partial x_0}, \frac{\partial S}{\partial y_0} \right) \tag{5}$$

where (X_0, Y_0) is the new estimate for the center of the pattern. A convenient and well known formula for computing the sum of squares is

$$S(x_0, y_0) = \sum_{j=1}^{J-1} \delta_j^2 - \frac{\left(\sum_{j=1}^{J-1} \delta_j \right)^2}{J-1}$$

The dependence of δ_j on (x_0, y_0) has been suppressed in the notation. We now compute the gradient of this function. Its x component is

$$\frac{\partial S}{\partial x_0} = 2 \sum_{j=1}^{J-1} \delta_j \frac{\partial \delta_j}{\partial x_0} - 2 \frac{\left(\sum_{j=1}^{J-1} \delta_j \right) \left(\sum_{j=1}^{J-1} \frac{\partial \delta_j}{\partial x_0} \right)}{J-1} \tag{6}$$

and its y component is

$$\frac{\partial S}{\partial y_0} = 2 \sum_{j=1}^{J-1} \delta_j \frac{\partial \delta_j}{\partial y_0} - 2 \frac{\left(\sum_{j=1}^{J-1} \delta_j \right) \left(\sum_{j=1}^{J-1} \frac{\partial \delta_j}{\partial y_0} \right)}{J-1}. \tag{7}$$

We need the partial derivatives for the δ_j. They can be computed from the formulas above for δ_j.

$$\begin{aligned}
\frac{\partial \delta_j}{\partial x_0} &= \frac{\partial \theta_{j+1}}{\partial x_0} - \frac{\partial \theta_j}{\partial x_0} \\
\frac{\partial \delta_j}{\partial y_0} &= \frac{\partial \theta_{j+1}}{\partial y_0} - \frac{\partial \theta_j}{\partial y_0}
\end{aligned} \tag{8}$$

These partial derivatives for the θ_j can be computed from the formulas above for θ_j.

$$\begin{aligned}
\frac{\partial \theta_j}{\partial x_0} &= \frac{\partial}{\partial x_0} \text{atan2}(y_j - y_0, x_j - x_0) \\
\frac{\partial \theta_j}{\partial y_0} &= \frac{\partial}{\partial y_0} \text{atan2}(y_j - y_0, x_j - x_0)
\end{aligned}$$

We now need the partial derivatives of atan2. For $x \neq 0$ they can be computed by using the chain rule with $\arctan(y/x)$, $\arctan(y/x) + 180^o$, and $\arctan(y/x) - 180^o$. Of course the addition of a constant has no affect on the derivative.

$$\begin{aligned}
\frac{\partial}{\partial x} \text{atan2}(y,x) &= -\frac{y}{x^2 + y^2} \\
\frac{\partial}{\partial y} \text{atan2}(y,x) &= \frac{x}{x^2 + y^2}
\end{aligned}$$

We can extend these formulas by continuity to the cases where $x = 0$ and $y \neq 0$ so that atan2 is differentiable over the whole plane except at the

origin. Now applying the chain rule with these formulas gives

$$\begin{aligned}\frac{\partial\theta_j}{\partial x_0} &= \frac{y_j - y_0}{(x_j - x_0)^2 + (y_j - y_0)^2} \\ \frac{\partial\theta_j}{\partial y_0} &= -\frac{x_j - x_0}{(x_j - x_0)^2 + (y_j - y_0)^2}\end{aligned} \tag{9}$$

We now have all the formulas needed to implement the gradient descent algorithm. We use the measured values, (x_j, y_j), for the location of the primordia in equation (9) to give us the partial derivatives of the angular coordinates θ_j. We substitute this into equation (8) to get the partial derivatives of the divergence angles δ_j. We substitute this into equations (6) and (7) to get the partial derivatives of the sums of squares S. And finally we substitute this into equation (5).

These calculations are too much to do by hand but they are actually quite easy to do on a desktop computer[7].

Appendix C

In this appendix we estimate the error of approximations (2), (3), and (4) in section 6. We let $\overline{\delta}$ be the mean of $\delta_1, \ldots, \delta_{J-1}$ and s be the standard deviation. Similarly $\overline{\delta}'$ denotes the mean of $\delta'_1, \ldots, \delta'_{J-1}$ and s' is the standard deviation.

Since divergence angles are differences between angular positions the scale of the differences between corresponding angular positions is about the same as the scale of the differences between corresponding divergence angles. There are at most a few hundred primordia in an apex and there is very little chance that corresponding divergence angles would differ by more than five times the sum of the standard deviations of the two sequences of divergence angles. So it is very unlikely that experimental error in the measurement of a primordium's position would cause the angular position to differ by more than $5(s + s')$. In most cases it will differ by much less but here we will make a very conservative estimate. The differences between the sums $\sum_{j=1}^{J-1}\delta_j$ and $\sum_{j=1}^{J-1}\delta'_j$ depends only the difference between the angular positions of (x_1, y_1), (x'_1, y'_1) and the difference between the angular positions of (x_J, y_J), (x'_J, y'_J). This gives us

$$\left|\sum_{j=1}^{J-1}\delta'_j - \sum_{j=1}^{J-1}\delta_j\right| \prec 10(s + s') \tag{10}$$

The symbol "$\prec$" is meant to indicate that it is very likely for the left hand side to be less than the right hand side.

A straight forward algebraic computation gives the equality

$$\begin{aligned}&\frac{\sum_{j=1}^{J-1}(\delta'_j - \overline{\delta})^2}{J-1} - \frac{\sum_{j=1}^{J-1}(\delta'_j - \overline{\delta}')^2}{J-1} \\ &= (\overline{\delta}' - \overline{\delta})^2 = \frac{1}{(J-1)^2}\left(\sum_{j=1}^{J-1}\delta'_j - \sum_{j=1}^{J-1}\delta_j\right)^2\end{aligned}$$

Combining this computation with inequality (10) just above gives

$$\begin{aligned}&\left|\frac{\sum_{j=1}^{J-1}(\delta'_j - \overline{\delta})^2}{J-1} - \frac{\sum_{j=1}^{J-1}(\delta'_j - \overline{\delta}')^2}{J-1}\right| \\ &\qquad \prec \frac{100(s + s')^2}{(J-1)^2}\end{aligned} \tag{11}$$

This is our estimate for the error of approximation (2) in section 6. Keeping s, s' small and J large keeps this error small.

Another straight forward algebraic computation shows that

$$\begin{aligned}&\frac{\sum_{j=1}^{J-1}(\delta'_j - \delta_j)^2}{J-1} - \frac{\sum_{j=1}^{J-1}(\delta'_j - \overline{\delta})^2}{J-1} \\ &= \frac{1}{J-1}\sum_{j=1}^{J-1}((\delta'_j - \delta_j) + (\delta'_j - \overline{\delta}))(\overline{\delta} - \delta_j)\end{aligned}$$

Taking the absolute value of both sides and applying the triangle inequality in a straight forward manner several times gives us

$$\begin{aligned}&\left|\frac{\sum_{j=1}^{J-1}(\delta'_j - \delta_j)^2}{J-1} - \frac{\sum_{j=1}^{J-1}(\delta'_j - \overline{\delta})^2}{J-1}\right| \\ &\leq \frac{1}{J-1}\sum_{j=1}^{J-1}(|\delta'_j - \delta_j| + |\delta'_j - \overline{\delta}|)|\overline{\delta} - \delta_j|\end{aligned}$$

[7] A sample C code that implements this algorithm along with instructions for its use is at http://math.smith.edu/~phyllo/Research/findcenter/findcenter.html

Another application of the triangle inequality gives us

$$|\delta'_j - \overline{\delta}| \leq |\delta'_j - \overline{\delta}'| + |\overline{\delta}' - \overline{\delta}|$$

Therefore

$$\left| \frac{\sum_{j=1}^{J-1}(\delta'_j - \delta_j)^2}{J-1} - \frac{\sum_{j=1}^{J-1}(\delta'_j - \overline{\delta})^2}{J-1} \right| \leq$$

$$\frac{1}{J-1}\sum_{j=1}^{J-1}(|\delta'_j - \delta_j| + |\delta'_j - \overline{\delta}'| + |\overline{\delta}' - \overline{\delta}|)|\overline{\delta} - \delta_j|$$

As we have already stated it is very unlikely for δ'_j and δ_j to differ by more than $5(s+s')$. It is also very unlikely for δ_j and $\overline{\delta}$ to differ by more than $5s$ or for δ'_j and $\overline{\delta}$ to differ by more than $5s'$. And using inequality (10) above gives

$$|\overline{\delta}' - \overline{\delta}| \prec \frac{10(s+s')}{J-1}$$

Therefore

$$\left| \frac{\sum_{j=1}^{J-1}(\delta'_j - \delta_j)^2}{J-1} - \frac{\sum_{j=1}^{J-1}(\delta'_j - \overline{\delta})^2}{J-1} \right|$$

$$\prec \frac{1}{J-1}\sum_{j=1}^{J-1}\left(5(s+s') + 5s' + \frac{10(s+s')}{J-1}\right)5s$$

Since there are $J-1$ terms in the sum this simplifies to

$$\left| \frac{\sum_{j=1}^{J-1}(\delta'_j - \delta_j)^2}{J-1} - \frac{\sum_{j=1}^{J-1}(\delta'_j - \overline{\delta})^2}{J-1} \right| \tag{12}$$

$$\prec 25s\left(s + 2s' + \frac{10(s+s')}{J-1}\right)$$

This is an estimate for the error of approximation (3) in section 6.

Combining the triangle inequality with inequalities (12) and (13) we get

$$\left| \frac{\sum_{j=1}^{J-1}(\delta'_j - \delta_j)^2}{J-1} - \frac{\sum_{j=1}^{J-1}(\delta'_j - \overline{\delta})^2}{J-1} \right| \tag{13}$$

$$\prec \frac{100(s+s')^2}{(J-1)^2} + 25s\left(s + 2s' + \frac{10(s+s')}{J-1}\right)$$

The left hand side of this inequality contains the two terms in expression (4) of section 6. We see that the smaller s and s' are the more confident we can be that the left and right hand sides of (4) are close to each other. The coefficients may seem large but remember that we are being very conservative here. The key point is that the difference between the left and right hand sides of (4) has very little chance of being larger than this homogeneous quadratic polynomial in s and s'. Therefore the smaller we can make s and s' be the more confident we can be that the left and right hand sides of (4) are close to each other.

If we could be lucky enough to get $s = s' = 0$ then the left and right hand sides of (4) would be equal. Further if $s' = 0$ the right hand side of (4) would be zero. Therefore the left hand side would be zero as well. This means the two sequences $\delta'_1, \ldots, \delta'_{J-1}$ and $\delta_1, \ldots, \delta_{J-1}$ would be the same.

With experimental errors in the measurements of naturally occurring phyllotactic patterns it is very unlikely we would get $s = s' = 0$ but using the minimal variation center to keep these standard deviations as small as we can reduces the amount of separation between the sums $\sum_{j=1}^{J-1}(\delta'_j - \delta_j)^2$ and $\sum_{j=1}^{J-1}(\delta'_j - \overline{\delta}')^2$. Since the minimal variation center minimizes the sum $\sum_{j=1}^{J-1}(\delta'_j - \overline{\delta}')^2$ it approximately minimizes the sum $\sum_{j=1}^{J-1}(\delta'_j - \delta_j)^2$. This means we have reduced the distance between the two sequences of divergence angles $\delta'_1, \ldots, \delta'_{J-1}$ and $\delta_1, \ldots, \delta_{J-1}$.

Appendix D

In this appendix we compute the partial derivatives of the function $S(\phi_0, \psi_0, x_0, y_0)$ in section 8. The formula for gradient descent is

$$(\Phi_0, \Psi_0, X_0, Y_0)$$

$$= (\phi_0, \psi_0, x_0, y_0) - \epsilon\left(\frac{\partial S}{\partial \phi_0}, \frac{\partial S}{\partial \psi_0}, \frac{\partial S}{\partial x_0}, \frac{\partial S}{\partial y_0}\right)$$

Since the values of (x_j, y_j) as defined in section 8 do not depend on x_0 or y_0 the computation of the partial derivatives with respect to x_0 and y_0 proceeds just as it did in appendix B. We only need to compute the partial derivatives with re-

spect to ϕ_0 and ψ_0. We begin with

$$\frac{\partial S}{\partial \phi_0} = 2\sum_{j=1}^{J-1} \delta_j \frac{\partial \delta_j}{\partial \phi_0} - 2\frac{\left(\sum_{j=1}^{J-1} \delta_j\right)\left(\sum_{j=1}^{J-1} \frac{\partial \delta_j}{\partial \phi_0}\right)}{J-1}$$

$$\frac{\partial S}{\partial \psi_0} = 2\sum_{j=1}^{J-1} \delta_j \frac{\partial \delta_j}{\partial \psi_0} - 2\frac{\left(\sum_{j=1}^{J-1} \delta_j\right)\left(\sum_{j=1}^{J-1} \frac{\partial \delta_j}{\partial \psi_0}\right)}{J-1}$$

We need $\frac{\partial \delta_j}{\partial \phi_0}$ and $\frac{\partial \delta_j}{\partial \psi_0}$. Like in appendix B

$$\begin{aligned} \frac{\partial \delta_j}{\partial \phi_0} &= \frac{\partial \theta_{j+1}}{\partial \phi_0} - \frac{\partial \theta_j}{\partial \phi_0} \\ \frac{\partial \delta_j}{\partial \psi_0} &= \frac{\partial \theta_{j+1}}{\partial \psi_0} - \frac{\partial \theta_j}{\partial \psi_0} \end{aligned}$$

Applying the chain rule to

$$\theta_j = atan2(y_j - y_0, x_j - x_0)$$

gives

$$\frac{\partial \theta_j}{\partial \phi_0} = \frac{(x_j - x_0)\frac{\partial y_j}{\partial \phi_0} - (y_j - y_0)\frac{\partial x_j}{\partial \phi_0}}{(x_j - x_0)^2 + (y_j - y_0)^2}$$

$$\frac{\partial \theta_j}{\partial \psi_0} = \frac{(x_j - x_0)\frac{\partial y_j}{\partial \psi_0} - (y_j - y_0)\frac{\partial x_j}{\partial \psi_0}}{(x_j - x_0)^2 + (y_j - y_0)^2}$$

We compute $\partial x_j/\partial \phi_0, \partial y_j/\partial \phi_0, \partial x_j/\partial \psi_0, \partial y_j/\partial \psi_0$ using the basic rules for finding derivatives.

$$\begin{aligned} \frac{\partial x_j}{\partial \phi_0} &= -u_j \cos(\phi_0) - \sin(\phi_0)(v_j \cos(\psi_0) + w_j \sin(\psi_0)) \\ \frac{\partial y_j}{\partial \phi_0} &= 0 \\ \frac{\partial x_j}{\partial \psi_0} &= -v_j \cos(\phi_0)\sin(\psi_0) + w_j \cos(\phi_0)\cos(\psi_0) \\ \frac{\partial y_j}{\partial \psi_0} &= -v_j \cos(\psi_0) - w_j \sin(\psi_0) \end{aligned}$$

These formulas allow us to compute $\partial S/\partial \phi_0$ and $\partial S/\partial \psi_0$[8].

[8] A sample C code that implements this algorithm along with instructions for its use is at http://math.smith.edu/~phyllo/Research/findcenter/findcenter.html